# Strain Effects in Narrow-Bandwidth Manganites: The Case of Epitaxial $Eu_{0.7}Sr_{0.3}MnO_3$ Thin Films

Eun Ju Moon,[1,*] David J. Keavney,[2] and Steven J. May[1,†]

[1]*Department of Materials Science & Engineering, Drexel University, Philadelphia, Pennsylvania 19104, USA*

[2]*Advanced Photon Source, Argonne National Laboratory, Argonne, Illinois 60439, USA*

(Received 27 February 2014; revised manuscript received 23 May 2014; published 26 June 2014)

We have investigated the strain-dependent magnetic properties of epitaxial narrow-bandwidth manganite, $Eu_{0.7}Sr_{0.3}MnO_3$ (ESMO), thin films on various substrates traversing from compressive (−2.4%) to tensile (+1.5%) strain. The stoichiometry and crystalline quality of the films were confirmed with diffraction and spectroscopic-based characterization. Using field- and temperature-dependent magnetometry, we find that the epitaxial strain acts to suppress the ferromagnetic state, although films under compressive strain retain a greater propensity for ferromagnetic behavior. However, temperature-dependent resistivity reveals that ESMO thin films exhibit a ferromagnetic insulating state in contrast to wide-bandwidth $La_{0.7}Sr_{0.3}MnO_3$ films under a comparable strain. The combination of a highly strain-dependent ferromagnetic state and robust insulating behavior may offer novel applications in spin filtering, sensing, or electronics.

DOI: 10.1103/PhysRevApplied.1.054006

## I. INTRODUCTION

Manganese-based perovskite oxides, $A_{1-x}A'_xMnO_3$ ($A$ = La, Pr, Nd, Sm, Eu, $A'$ = Ca, Sr, Ba), are actively synthesized and investigated in order to understand their structural behavior, magnetic properties, and charge or orbital ordering which are often coupled, leading to complex physical properties [1–4]. Depending on the $A$-site composition, the manganites can exhibit double-exchange or superexchange interactions between adjacent $Mn^{3+}$ and $Mn^{4+}$ cations, leading to a variety of magnetic states including nearly half-metallic ferromagnetism, multiple antiferromagnetic spin structures, spin-glass behavior, and canted antiferromagnetism [5–9]. This array of magnetic functionalities has generated considerable interest for applications in spintronics, electronics, and sensing [10–14].

A critical parameter in determining magnetic coupling is the Mn $e_g$ electronic bandwidth, which is coupled to lattice distortions that arise due to deviations from the ideal perovskite structure, most critically distortions and rotations of the $MnO_6$ octahedra [15–19]. In narrow-bandwidth manganites such as $Pr_{1-x}Ca_xMnO_3$ [20,21], $Sm_{1-x}Sr_xMnO_3$ [22], and $Nd_{1-x}Sr_xMnO_3$ [23], competing magnetic and electronic phases often reside in close energetic proximity. In such cases, the dominant magnetic and electronic phase can become unstable under the application of a variety of external stimuli, including magnetic, electrical, pressure, and light [24–28]. This functional response points to several possible applications in electronic devices and sensors.

$Eu_{1-x}Sr_xMnO_3$ exhibits a strongly distorted orthorhombic structure due to the relatively small size of the Eu ion (i.e., a reduced tolerance factor compared to $La_{1-x}Sr_xMnO_3$). Previous studies of bulk $Eu_{1-x}Sr_xMnO_3$ have revealed rich magnetic behavior, in which the stability of the magnetic order is extremely sensitive to external magnetic fields and the cation composition ($x$) [29–33]. The $Eu_{0.7}Sr_{0.3}MnO_3$ composition is of particular interest compared to other narrow-bandwidth $A_{0.7}Sr_{0.3}MnO_3$ compounds, as bulk $Sm_{0.7}Sr_{0.3}MnO_3$ is ferromagnetic while $Gd_{0.7}Sr_{0.3}MnO_3$ is antiferromagnetic [21,34]. Therefore, $Eu_{0.7}Sr_{0.3}MnO_3$ resides near a ferromagnetic or antiferromagnetic phase boundary, the stability of which is determined by structural distortions, making it an excellent candidate for investigating the use of epitaxial strain to alter magnetically ordered phases.

Despite this, the magnetic and electronic behavior of epitaxially strained $Eu_{0.7}Sr_{0.3}MnO_3$ thin films has yet to be reported even though epitaxial thin films can present quite different properties from those of isocompositional bulk materials, as strain, interfacial structural coupling, and reduced dimensionality can significantly alter behavior in complex oxides [35–43]. Here, we show that the behavior of the narrow-bandwidth manganite, $Eu_{0.7}Sr_{0.3}MnO_3$ (ESMO), exhibits an enhanced sensitivity to strain compared to the well-studied $La_{0.7}Sr_{0.3}MnO_3$ (LSMO) system. In particular, we find that a moderate tensile strain (1.5%) suppresses the ferromagnetic ground state. In an additional difference to wide-bandwidth manganite films, ESMO films retain insulating behavior

*em582@drexel.edu
†smay@coe.drexel.edu

 

independent of the strain state. Thus, films grown on relatively lattice-matched substrates are ferromagnetic and insulating, an uncommon combination of properties that may be useful for devices or sensors.

## II. EXPERIMENTAL METHODS

ESMO thin films are grown with oxide molecule beam epitaxy by an interrupted epitaxial growth mode on $SrTiO_3$ (STO, lattice mismatch $\epsilon \sim 1.52\%$), $(LaAlO_3)_{0.3}(Sr_2AlTaO_6)_{0.7}$ (LSAT, approximately 0.58%), $LaAlO_3$ (LAO, approximately $-1.47\%$), and $SrLaAlO_4$ (SLAO, approximately $-2.39\%$) substrates. During deposition, the substrate temperature is held at approximately 620 °C, and the ozone-to-oxygen mixture (approximately 5/95%) is sourced to the substrate at a rate that yields a chamber pressure of approximately $8 \times 10^{-6}$ Torr. Growth is monitored by *in situ* reflection high-energy electron diffraction (RHEED). The atomic fluxes for the cation deposition are calibrated using Rutherford backscattering spectroscopy (RBS) and x-ray reflectivity (XRR). Film thickness and smooth surface morphology are confirmed by XRR. The thickness of all ESMO films in this study is 40 unit cells (u.c.). XRD measurements are taken around the (0 0 2) (pseudocubic notation) truncation rod of the film with a Rigaku Smartlab diffractometer, equipped with a parabolic mirror and a two-bounce monochromator on the incident beam. The same instrument is used to measure a reciprocal space map (RSM) around the (1 0 3) truncation rod. Resonant soft x-ray spectroscopy was performed at the beam line 4-ID-C of the Advanced Photon Source at Argonne National Laboratory in total electron yield mode to probe the Eu $M_5$ and Mn $L_{2,3}$ edges at 300 K. Magnetic properties are measured in a Quantum Design physical-property measurement system (PPMS) with vibrating sample magnetometry.

## III. RESULTS AND DISCUSSION

Figure 1(a) shows a RHEED image of a 40-u.c.-thick ESMO film on STO. Well-defined streaks appear at the (0 1), (0 0), and (0 $\bar{1}$) reflections confirming the smooth surface of the epitaxial ESMO thin film. The corresponding XRR data are shown in Fig. 1(b). The XRR data are fit with the GENX program; the data fit well to a model with a uniform scattering length density throughout the film and an abrupt film-substrate interface. Figure 1(c) shows XRD measurements taken around the (0 0 2) truncation rod of the ESMO films grown on various substrates. The film peaks exhibit noticeable shifts from the bulk ESMO lattice constant ($a_{\text{pseudocubic}} \sim 3.846$ Å, in bulk) [29]. The out-of lattice parameters of the films are displayed in Fig. 1(d), obtained from Fig. 1(c). Based on the positions of the ESMO (0 0 2) and the substrate of STO, LSAT, and LAO (0 0 2) and SLAO (0 0 6) reflections, the pseudocubic lattice parameters of the

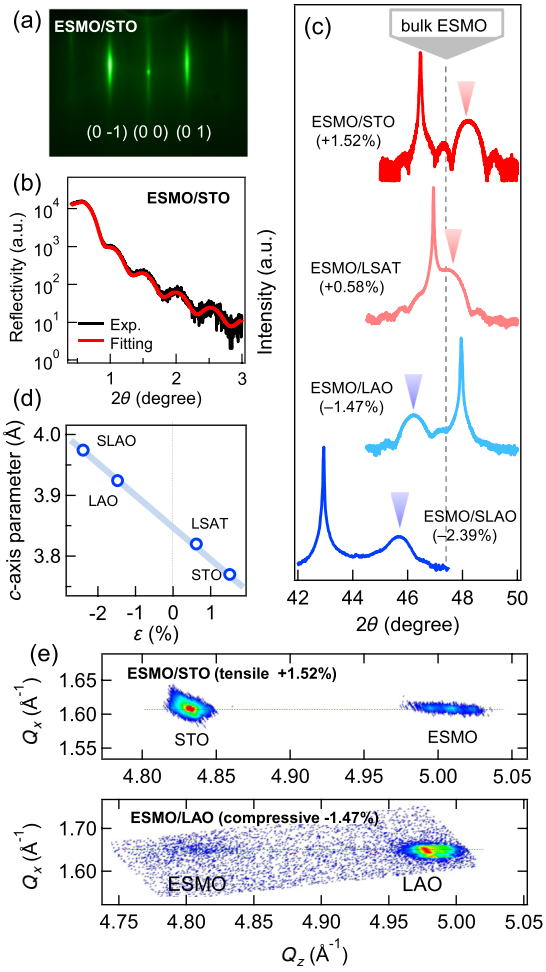


FIG. 1. (a) RHEED image of the 40 u,c, ESMO film on STO after growth. (b) Corresponding XRR of the ESMO/STO film. (c) XRD data for ESMO films on the different substrates. (d) The out-of-plane lattice parameters of the films as a function of strain. (e) Reciprocal space map measured from a ESMO film grown on STO (top) and on LAO (bottom) around the (1 0 3) reflection.

ESMO thin films are shifted in response to the various strain states. To confirm the coherent strain state of ESMO, a reciprocal space map (RSM) around the (1 0 3) Bragg peak for the ESMO film on STO and LAO is shown in Fig. 1(e). The red horizontal line indicates the in-plane ($Q_x$) position of the ESMO film and STO, which exhibit the same in-plane lattice constant, confirming that the film is coherently strained.

To further examine the stoichiometry of the films, we used RBS to confirm the cation composition and x-ray absorption spectroscopy (XAS) to investigate the Eu and Mn valence states. Figure 2(a) displays the RBS spectrum measured from the film grown on STO and a simulated spectrum for the $Eu_{0.7}Sr_{0.3}MnO_3$ composition. Good agreement between the data and simulation indicates that the film has the target stoichiometry. Figure 2(b) shows the Eu

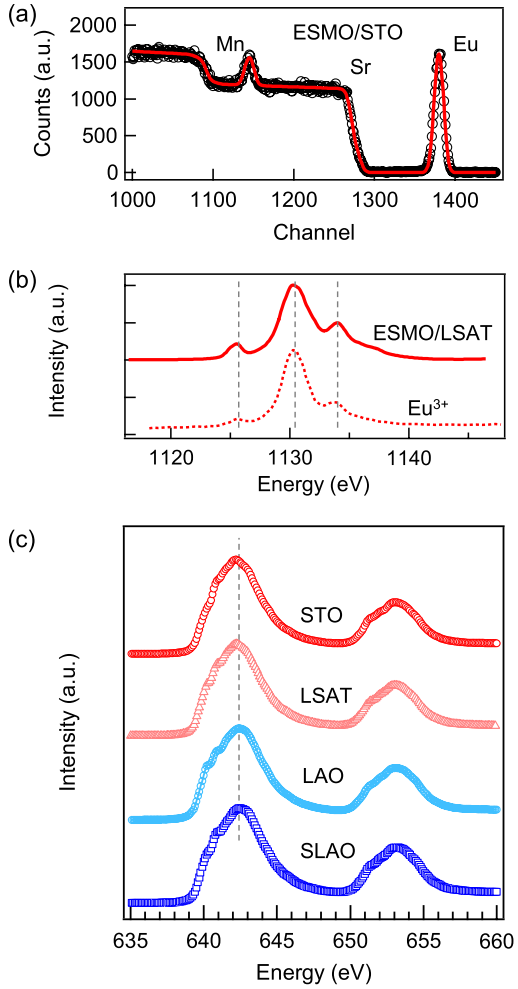


FIG. 2. (a) RBS data (open symbols) and simulations (solid red curves) of the ESMO film grown on STO. (b) XAS data of the Eu $M_5$ edge measured at 100 K, plotted with a previously reported experimental $Eu^{3+}$ spectrum for comparison (data from Ref. [44]). (c) XAS data of the Mn $L_{2,3}$ edge for ESMO films on four different substrates measured at 300 K.

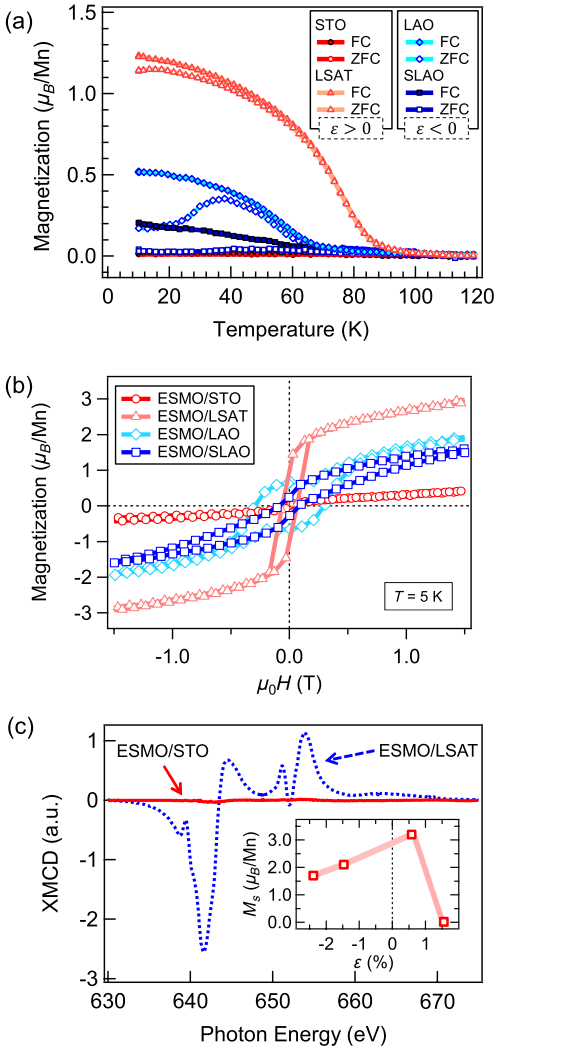


FIG. 3. (a) Temperature-dependent magnetization ($M$-$T$) in ZFC and FC modes under 0.05 T of ESMO grown on STO, LSAT, LAO, and SLAO. (b) Magnetization loops ($M$-$H$) taken at 5 K between −1.5 and 1.5 T. (c) XMCD data of ESMO films on STO (red solid line) and LSAT (blue dashed line) at 10 K under 300 Oe. Inset: Saturation magnetization at 5 K as a function of lattice mismatch.

$M_5$-edge XAS spectrum measured from a ESMO film on LSAT. It is clearly shown that the Eu $M_5$-edge spectrum of the ESMO thin film is in good agreement with that of $Eu^{3+}$, as previously reported for $Eu_2O_3$ (a dashed curve) [44]. Figure 2(c) shows the Mn $L_{2,3}$-edge XAS spectra probing the unoccupied Mn $3d$ states via the $2p$-$3d$ dipole transition for the four different strained ESMO thin films. The spectra from the ESMO thin films display the same qualitative characteristics, confirming the same nominal Mn valence state in all of the films. Additionally, the $L_3$ peak position is consistent with previous reports of $A_{0.7}A'_{0.3}MnO_3$ samples [45,46], providing additional validation of the $x = 0.3$ stoichiometry.

The temperature-dependent field-cooled (FC) and zero-field-cooled (ZFC) magnetizations measured in a magnetic field of 0.05 T applied parallel to the film are shown in Fig. 3(a). The Curie temperatures, $T_C$, are approximately 90 K for ESMO/LSAT, 80 K for ESMO/LAO (under 0.15 T and 70 K under 0.05 T), and 60 K for ESMO/SLAO. Note that the $T_C$ of bulk ESMO is approximately 65 K when measured at low fields; however, magnetization can persist to temperatures above 100 K in fields greater than 1 T [29,30]. Interestingly, the ferromagnetic state of the film on STO is suppressed, leading to a negligible magnetization as a function of temperature. We attribute this evolution in $T_C$ to the biaxial epitaxial strains. As shown in Fig. 3(a), a large irreversibility between ZFC and FC magnetizations is observed for compressive strained ESMO on LAO and SLAO. During the FC process, the ESMO/LAO magnetization increases rapidly below $T_C$, behavior that we also find in ESMO/SLAO and ESMO/LSAT. Additionally, the

FC behavior is qualitatively the same for bulk ESMO and these films [29,32].

We measure magnetic hysteresis loops ($M$-$H$) at 5 K, as shown in Fig 3(b). The film grown on STO exhibits negligible magnetization. In contrast, the film on LSAT exhibits a hysteresis loop consistent with typical ferromagnetic behavior in manganites and a saturation magnetization of approximately 3.3 $\mu_B$/Mn similar to that of bulk ESMO [30]. In the films under compressive strain, the magnetization continuously increases with the applied field with the presence of a clear remnant magnetization, indicative of a ferromagnetic state, with saturation magnetizations of approximately 1.8 and approximately 2.1 $\mu_B$/Mn for SLAO and LAO, respectively.

In order to confirm the abrupt suppression of magnetization between ESMO films on LSAT and on STO, shown in Figs. 3(a)–3(b), we perform an element-selective XMCD, in which the differences in the absorption of right and left circularly polarized x rays are measured at the Mn $L$ edge. Figure 3(c) shows the Mn $2p$ $(\rightarrow 3d)$ XMCD spectra of ESMO grown on the two substrates measured at 10 K under 300 Oe. The film grown on STO exhibits negligible dichroism signal. In contrast, ESMO on LSAT exhibits a clear XMCD signal. This result is consistent with the magnetization data in Fig. 3(a) showing the negligible magnetization from the ESMO on STO and the typical ferromagnetic behavior in manganites from the film on LSAT. This result is quite different from the behavior observed in LSMO, which remains ferromagnetic (albeit with a reduced $T_C$) even in the presence of over 3% tensile strain [35,47].

The inset to Fig. 3(c) shows the trend of saturation magnetization ($M_s$) as a function of lattice mismatch between the films and substrates. The thin film on LSAT, the least strained of the films, exhibits the highest $M_s$, which becomes suppressed as ESMO films are subjected to increasing strain (either compressive or tensile). This indicates that the presence of the lattice mismatch provides a means to tune the magnetization and the magnetic ordering transition temperature. As shown in the inset of Fig. 3(c), the magnetic properties can be altered from weakly ferromagnetic, ferromagnetic, and paramagnetic with widely varying ordering temperatures through biaxial strain, which alters the $MnO_6$ rotations and distortions.

We next turn to the electronic transport as the magnetic and electronic properties are strongly coupled in mixed-valence manganites. Figure 4(a) shows the temperature dependence of the resistivity, $\rho(T)$, of the ESMO films (40 u.c. thick) grown on four different substrates and LSMO films (20 u.c. on LSAT and 80 u.c. on STO) on both STO (red solid line) and LSAT substrates. Four ESMO films exhibit insulating behavior with little difference between the ferromagnetic film on LSAT, weak ferromagnetic film on LAO and SLAO, and the paramagnetic film on STO. Below approximately 120 K the films become too insulating for our measurement capabilities. The resistivity exhibits simple Arrhenius behavior, following $\rho = \rho_0 e^{-E_A/k_B T}$, with an activation energy ($E_A$) of 150 meV. The electrical behavior of the films is in agreement with previous reports from bulk ESMO, except we note that below $T_C$ a decrease in resistivity is observed in bulk [29,48]. However, the value of resistivity reported in the ferromagnetic state remains above $10^4$ Ω cm, which is the upper limit of our measurement capabilities for films of this thickness. The insulating behavior in the ESMO films stands in contrast to LSMO grown on STO, which is under approximately the same magnitude of tensile strain as ESMO on LSAT. The LSMO/STO film shows typical metallic behavior associated with double-exchange ferromagnetism including an inflection in the resistivity near $T_C$.

The magnetoresistance (MR) of the ESMO films, shown in Fig. 4(b), exhibits strain-dependent trends similar to the magnetization. The MR data are obtained in a field of 7 T applied perpendicular to the plane of the film. Interestingly, the film on LSAT shows higher MR than the rest and that on LAO, SLAO, and STO, in order. This MR behavior is

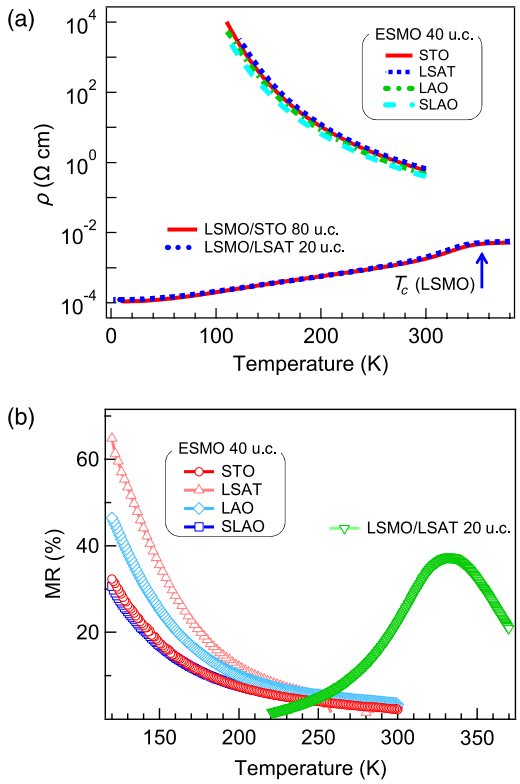


FIG. 4. (a) Temperature-dependent resistivity measured in zero magnetic field for ESMO films. For comparison, the resistivity of LSMO films grown on STO and LSAT is also presented. The blue arrow indicates the Curie temperature of the LSMO film on LSAT measured with magnetometry. (b) The corresponding MR $[(\rho_0 - \rho_{7T}) \times 100\%/\rho_0]$.

consistent with magnetization data in that the ferromagnetic samples tend to have the largest MR.

Finally, we comment on potential applications enabled by the novel combination of magnetic properties that are strongly dependent on epitaxial strain and insulating behavior observed in the ESMO films. This high sensitivity to lattice strain and robust insulating behavior distinguishes the narrow-bandwidth ESMO films from their wide-bandwidth LSMO counterparts, and may lead to unique applications in spintronics or sensing. Ferromagnetic insulators are the enabling material component for tunneling spin filters [49]; for instance, thin ferromagnetic $Sm_{0.75}Sr_{0.25}MnO_3$ layers have recently been utilized as spin-filtering tunnel barriers [50]. The use of ESMO as tunnel barriers could enable strain-dependent spin filtering in which the ability to tune the magnetic state of an insulating barrier via piezoelectric strain modification [51] would offer voltage-tunable spin injection. Additionally, strain-based control of magnetism in ESMO using piezoelectric substrates may lead to tunable microwave components such as filters or resonators [52,53].

## ACKNOWLEDGMENTS

We thank Leszek Wielunski and Boris Yakshinskiy for RBS measurements at the Laboratory for Surface Modification at Rutgers University and Yujun Xie for ESMO resistivity measurements. This work is supported by the U.S. Army Research Office under Grant No. W911NF-12-1-0132. Acquisition of the PPMS is supported by the U.S. Army Research Office under Grant No. W911NF-11-1-0283. Use of the Advanced Photon Source, an Office of Science User Facility operated for the U.S. Department of Energy (DOE) Office of Science by Argonne National Laboratory, was supported by the U.S. DOE under Contract No. DE-AC02-06CH11357.

[1] *Colossal Magnetoresistive Oxides*, edited by Y. Tokura (Gordon and Breach Publishers, Amsterdam, 2000), pp. 28–38 and 237–240; *Nanoscale Phase Separation and Colossal Magnetoresistance*, edited by E. Dagotto (Springer, Berlin, 2003), p. 357.

[2] S. Murakami and N. Nagaosa, Colossal magnetoresistance in manganites as a multicritical phenomenon, Phys. Rev. Lett. **90**, 197201 (2003).

[3] Y. Tokura and N. Nagaosa, Orbital physics in transition-metal oxides, Science **288**, 462 (2000).

[4] E. Dagotto, T. Hotta, and A. Moreo, Colossal magnetoresistant materials: The key role of phase separation, Phys. Rep. **344**, 1 (2001).

[5] Y. Tokura, Critical features of colossal magnetoresistive manganites, Rep. Prog. Phys. **69**, 797 (2006).

[6] G. H. Jonker and J. H. van Santen, Ferromagnetic compounds of manganese with perovskite structure, Physica **16**, 337 (1950).

[7] J. B. Goodenough, Theory of the role of covalence in the perovskite-type manganites $[La, M(II)]MnO_3$, Phys. Rev. **100**, 564 (1955).

[8] P. W. Anderson and H. Hasegawa, Considerations on double exchange, Phys. Rev. **100**, 675 (1955).

[9] P.-G. de Gennes, Effects of double exchange in magnetic crystals, Phys. Rev. **118**, 141 (1960).

[10] M. Bibes and A. Barthélémy, Oxide spintronics, IEEE Trans. Electron Devices **54**, 1003 (2007).

[11] T. Yajima, Y. Hikita, and H. Y. Hwang, A heteroepitaxial perovskite metal-base transistor, Nat. Mater. **10**, 198 (2011).

[12] L. Jiang, W. S. Choi, H. Jeen, S. Dong, Y. Kim, M.-G. Han, Y. Zhu, S. V. Kalinin, E. Dagotto, T. Egami, and H. N. Lee, Tunneling electroresistance induced by interfacial phase transitions in ultrathin oxide heterostructures, Nano Lett. **13**, 5837 (2013).

[13] Y. Xu, U. Memmert, and U. Hartmann, Magnetic field sensors from polycrystalline manganites, Sens. Actuators A **91**, 26 (2001).

[14] Ll. Balcells, E. Calvo, and J. Fontcuberta, Room-temperature anisotropic magnetoresistive sensor based on manganese perovskite thick films, J. Magn. Magn. Mater. **242–245**, 1166 (2002).

[15] P. G. Radaelli, G. Iannone, M. Marezio, H. Y. Hwang, S.-W. Cheong, J. D. Jorgensen, and D. N. Argyriou, Structural effects on the magnetic and transport properties of perovskite $A_{1-x}A'_xMnO_3$ $(x = 0.25, 0.30)$, Phys. Rev. B **56**, 8265 (1997).

[16] J.-S. Zhou and J. B. Goodenough, Orbital order-disorder transition in single-valent manganites, Phys. Rev. B **68**, 144406 (2003).

[17] A. J. Millis, P. B. Littlewood, B. I. Shraiman, Double exchange alone does not explain the resistivity of $La_{1-x}Sr_xMnO_3$, Phys. Rev. Lett. **74**, 5144 (1995).

[18] L. M. Rodriguez-Martinez and J. P. Attfield, Cation disorder and size effects in magnetoresistive manganese oxide perovskites, Phys. Rev. B **54**, R15622 (1996).

[19] C. H. Booth, F. Bridges, G. H. Kwei, J. M. Lawrence, A. L. Corenlius, and J. J. Neumeier, Direct relationship between magnetism and $MnO_6$ distortions in $La_{1-x}Ca_xMnO_3$, Phys. Rev. Lett. **80**, 853 (1998).

[20] Y. Tomioka, A. Asamitsu, H. Kuwahara, Y. Moritomo, and Y. Tokura, Magnetic-field-induced metal-insulator phenomena in $Pr_{1-x}Ca_xMnO_3$ with controlled charge-ordering instability, Phys. Rev. B **53**, R1689 (1996).

[21] C. Martin, A. Maignan, M. Hervieu, and B. Raveau, Magnetic phase diagrams of $L_{1-x}A_xMnO_3$ manganites ($L$ = Pr, Sm; $A$ = Ca, Sr), Phys. Rev. B **60**, 12191 (1999).

[22] V. Yu. Ivanov, A. A. Mukhin, V. D. Travkin, A. S. Prokhorov, and A. M. Balbashov, Phase $T$-$x$ diagram of $Sm_{1-x}Sr_xMnO_3$ single crystals $(0 < x < 0.8)$, J. Magn. Magn. Mater. **258–259**, 535 (2003).

[23] R. Kajimoto, H. Yoshizawa, H. Kawano, H. Kuwahara, Y. Tokura, K. Ohoyama, and M. Ohashi, Hole-concentration-induced transformation of the magnetic and orbital structures in $Nd_{1-x}Sr_xMnO_3$, Phys. Rev. B **60**, 9506 (1999).

[24] R. von Helmolt, J. Wecker, B. Holzapfel, L. Schultz, and K. Samwer, Giant negative magnetoresistance in perovskitelike $La_{2/3}Ba_{1/3}MnO_x$ ferromagnetic films, Phys. Rev. Lett. **71**, 2331 (1993).

[25] A. Asamitsu, Y. Tomioka, H. Kuwahara, and Y. Tokura, Current switching of resistive states in magnetoresistive manganites, Nature (London) **388**, 50 (1997).

[26] Y. Moritomo, H. Kuwahara, and Y. Tokura, Bandwidth- and doping-dependent pressure effects on the ferromagnetic transition in perovskite manganites, J. Phys. Soc. Jpn. **66**, 556 (1997).

[27] S. Singh, M. R. Fitzsimmons, T. Lookman, J. D. Thompson, H. Jeen, A. Biswas, M. A. Roldan, and M. Varela, Magnetic nonuniformity and thermal hysteresis of magnetism in a manganite thin film, Phys. Rev. Lett. **108**, 077207 (2012).

[28] R. Singla, A. Simoncig, M. Först, D. Prabhakaran, A. L. Cavalieri, and A. Cavalleri, Photoinduced melting of the orbital order in $La_{0.5}Sr_{1.5}MnO_4$ measured with 4-$fs$ laser pulses, Phys. Rev. B **88**, 075107 (2013).

[29] Y. M. Mukovskii, G. Hilscher, H. Michor, and A. M. Ionov, Magnetic properties, resistivity, and heat capacity of $EuMnO_3$ and $Eu_{0.7}A_{0.3}MnO_3$ ($A$ = Ca, Sr) compounds, J. Appl. Phys. **83**, 7163 (1998).

[30] Y. Tomioka, R. Kumai, T. Ito, and Y. Tokura, Magnetic and electronic properties of $Eu_{1-x}Sr_xMnO_3$ ($0.3 < x < 0.7$) single crystals, Phys. Rev. B **80**, 174414 (2009).

[31] A. Sundaresan, A. Maignan, and B. Raveau, Spin-glass state and magnetic-field-induced phenomena in distorted $Eu_{0.58}Sr_{0.42}MnO_3$ perovskite, Phys. Rev. B **55**, 5596 (1997).

[32] Y. Tadokoro, Y. J. Shan, T. Nakamura, and S. Nakamura, Crystal structure and characterizations of perovskite oxides $(Eu_{1-x}Sr_x)MnO_3$ ($0.0 \leq x \leq 0.5$), Solid State Ionics **108**, 261 (1998).

[33] G. J. Liu, J. R. Sun, C. M. Xiong, D. J. Wang, Y. W. Xie, H. W. Zhang, T. Y. Zhao, and B. G. Shen, Heat capacity at the field-induced ferromagnetic transition in $Eu_{0.58}Sr_{0.42}MnO_3$, Appl. Phys. Lett. **87**, 182502 (2005).

[34] J. P. Zhou, J. T. McDevitt, J. S. Zhou, H. Q. Yin, J. B. Goodenough, Y. Gim, and Q. X. Jia, Effect of tolerance factor and local distortion on magnetic properties of the perovskite manganites, Appl. Phys. Lett. **75**, 1146 (1999).

[35] C. Adamo, X. Ke, H. Q. Wang, H. L. Xin, T. Heeg, M. E. Hawley, W. Zander, J. Schubert, P. Schiffer, D. A. Muller, L. Maritato, and D. G. Schlom, Effect of biaxial strain on the electrical and magnetic properties of (001) $La_{0.7}Sr_{0.3}MnO_3$ thin films, Appl. Phys. Lett. **95**, 112504 (2009).

[36] Y. Takamura, R. V. Chopdekar, E. Arenholz, and Y. Suzuki, Control of the magnetic and magnetotransport properties of $La_{0.67}Sr_{0.33}MnO_3$ thin films through epitaxial strain, Appl. Phys. Lett. **92**, 162504 (2008).

[37] J. M. Rondinelli, S. J. May, and J. W. Freeland, Control of octahedral connectivity in perovskite oxide heterostructures: An emerging route to multifunctional materials discovery, MRS Bull. **37**, 261 (2012).

[38] A. V. Boris, Y. Matiks, E. Benckiser, A. Frano, P. Popovich, V. Hinkov, P. Wochner, M. Castro-Colin, E. Detemple, V. K. Malik, C. Bernhard, T. Prokscha, A. Suter, Z. Salman, E. Morenzoni, G. Cristiani, H.-U. Habermeier, and B. Keimer, Dimensionality control of electronic phase transitions in nickel-oxide superlattices, Science **332**, 937 (2011).

[39] A. Goyal, M. Rajeswari, R. Shreekala, S. E. Lofland, S. M. Bhagat, T. Boettcher, C. Kwon, R. Ramesh, and T. Venkatesan, Material characteristics of perovskite manganese oxide thin films for bolometric applications, Appl. Phys. Lett. **71**, 2535 (1997).

[40] W. Prellier, M. Rajeswari, T. Venkatesan, and R. Greene, Effects of annealing and strain on $La_{1-x}Ca_xMnO_3$ thin films: A phase diagram in the ferromagnetic region, Appl. Phys. Lett. **75**, 1446 (1999).

[41] A. K. Pradhan, D. R. Sahu, B. Roul, and Y. Feng, $La_{1-x}Ba_xMnO_3$ epitaxial thin films by pulsed-laser deposition: A consequence of strain stabilization, Appl. Phys. Lett. **81**, 3597 (2002).

[42] E. J. Moon, J. M. Rondinelli, N. Prasai, B. A. Gray, M. Kareev, J. Chakhalian, and J. L. Cohn, Strain-controlled band engineering and self-doping in ultrathin $LaNiO_3$ films, Phys. Rev. B **85**, 121106(R) (2012).

[43] E. J. Moon, B. A. Gray, M. Kareev, J. Liu, S. G. Altendorf, F. Strigari, L. H. Tjeng, J. W. Freeland, and J. Chakhalian, Strain-dependent transport properties of the ultra-thin correlated metal, $LaNiO_3$, New J. Phys. **13**, 073037 (2011).

[44] Hangil Lee, J.-Y. Kim, K.-J. Rho, B.-G. Park, and J.-H. Park, Temperature dependent phase transition of EuO on MgO(100), J. Appl. Phys. **102**, 053903 (2007).

[45] T. Y. Cheng, C. C. Hsieh, J. Y. Juang, J.-Y. Lin, K. H. Wu, T. M. Wen, Y. S. Gou, and C. H. Hsu, The magneto-transport properties of epitaxial $La_{0.7}Sn_{0.3}MnO_3$ manganite thin films, Physica (Amsterdam) **365B**, 141 (2005).

[46] M. Huijben, L. W. Martin, Y.-H. Chu, M. B. Holcomb, P. Yu, G. Rijnders, D. H. A. Blank, and R. Ramesh, Critical thickness and orbital ordering in ultrathin $La_{0.7}Sr_{0.3}MnO_3$ films, Phys. Rev. B **78**, 094413 (2008).

[47] Y. Konishi, Z. Fang, M. Izumi, T. Manako, M. Kasai, H. Kuwahara, M. Kawasaki, K. Terakura, and Y. Tokura, Orbital-state-mediated phase-control of manganites, J. Phys. Soc. Jpn. **68**, 3790 (1999).

[48] L. I. Koroleva and R. Szymczak, Ferromagnetic-antiferromagnetic state in manganites, J. Phys. Chem. Solids **64**, 1565 (2003).

[49] J. S. Moodera, T. S. Santos, and T. Nagahama, The phenomena of spin-filter tunnelling, J. Phys. Condens. Matter **19**, 165202 (2007).

[50] B. Prasad, M. Egilmez, F. Schoofs, T. Fix, M. E. Vickers, W. Zhang, J. Jian, H. Wang, and M. G. Blamire, Nanopillar spin filter tunnel junctions with manganite barriers, Nano Lett. **14**, 2789 (2014).

[51] K. Dörr, O. Bilani-Zeneli, A. Herklotz, A. D. Rata, K. Boldyreva, J.-W. Kim, M. C. Dekker, K. Nenkov, L. Schultz, and M. Reibold, A model system for strain effects: Epitaxial magnetic films on a piezoelectric substrate, Eur. Phys. J. B **71**, 361 (2009).

[52] Y. K. Fetisov and G. Srinivasan, Electric field tuning characteristics of a ferrite-piezoelectric microwave resonator, Appl. Phys. Lett. **88**, 143503 (2006).

[53] N. Li, M. Liu, Z. Zhou, N. X. Sun, D. V. B. Murthy, G. Srinivasan, T. M. Klein, V. M. Petrov, and A. Gupta, Microstructural and ferromagnetic resonance properties of epitaxial nickel ferrite films grown by chemical vapor deposition, Appl. Phys. Lett. **99**, 192502 (2011).